Bioresource Technology 108 (2012) 264–273

Contents lists available at SciVerse ScienceDirect

Bioresource Technology

journal homepage: www.elsevier.com/locate/biortech

System characteristics and performance evaluation of a trailer-scale downdraft gasifier with different feedstock

Elango Balu, J.N. Chung *

Department of Mechanical and Aerospace Engineering, University of Florida, Gainesville, FL 32611, USA

ARTICLE INFO

Article history:
Received 19 November 2011
Received in revised form 20 December 2011
Accepted 20 December 2011
Available online 8 January 2012

Keywords:
Trailer-scale
Downdraft gasifer
Multiple feedstock
Equilibrium model
Bioenegy

ABSTRACT

The main objective of this study is to investigate the thermal profiles of a trailer-scale gasifier in different zones during the course of gasification and also to elaborate on the design, characteristics and performance of the gasification system using different biomass feedstock. The purpose is to emphasize on the effectiveness of distributed power generation systems and demonstrate the feasibility of such gasification systems in real world scenarios, where the lingo-cellulosic biomass resources are widely available and distributed across the board. Experimental data on the thermal profiles with respect to five different zones in the gasifier and a comprehensive thermal–chemical equilibrium model to predict the syngas composition are presented in detail. Four different feedstock-pine wood, horse manure, red oak, and cardboard were evaluated. The effects of C, H, O content variations in the feedstock on the thermal profiles, and the efficiency and viability of the trailer-scale gasifier are also discussed.

1. Introduction

The need for sustainable alternatives to oil has been of deep concern to the industrial countries due to the rising cost of oil. As a result, many nations face significant energy security challenges stemming from their dependence on imported oil. To achieve future energy security and independence and in the long run to prepare for the post-oil energy resources, biomass is considered as one of the most important primary, renewable energy resources in a projected sustainable energy future. A recent US NSF-DOE workshop report (Huber, 2007) concluded that biofuels produced from lignocellulosic biomass can significantly reduce US dependence on foreign oil, create new jobs, improve rural economics, reduce greenhouse emissions, and ensure national security. Furthermore, the report emphasized that the key bottleneck for lignocellulosic-derived biofuels is the lack of technology for the efficient conversion of biomass into biofuels. As a result, advanced technologies are needed to replace fossil fuels with renewable energy resources.

Lignocellulosic biomass is the fibrous, woody, and generally inedible portion of the plants that are mostly composed of hemicellulose and lignin. So, lignocellulosic biomass is non-food based and does not compete with the food crops that are basically cellulosic biomass. Most biomass materials are widely available in many parts of the world. As it is abundant, environmentally friendly and renewable, the potential of biomass to help meet the world energy demand has been widely recognized. Thermochemical gasification is likely to be the most cost effective conversion process. Biomass gasification is one of the highly effective technologies for thermo–chemical conversion. Therefore, biomass is considered as one of the most promising renewable energy sources. In a thermodynamic study, (Corradetti and Desideri, 2007) found that the hydrogen fuel can be produced from woody biomass gasification coupled with steam-methane reforming and water gas shift reaction in a large-scale industrial plant with an efficiency of 62% that is comparable with those of other existing process technologies. They also reported that an overall efficiency of 44% can be obtained for power production through a gas-steam combined cycle using woody biomass gasification as the energy source.

According to (Ruan et al., 2008) currently large-scale biomass energy production systems including cellulosic ethanol, gasification, and pyrolysis facilities experience technical and economic hurdles. Compared with these large-scale systems, small decentralized and distributed biomass energy production systems could offer advantages including lower capital costs, lower feedstock costs, simplified transportation and logistics, and higher returns for biomass producers. These small-scale distributed systems can directly utilize regional biomass supplies that are practical and economically viable from energy saving consideration. In this paper, the main objective is aimed at presenting a sound scientific, engineering, and technological solution for converting lignocellulosic biomass, as well as agricultural and forest residues to clean

* Corresponding author. Tel.: +1 352 392 9607; fax: +1 352 392 1071.
E-mail address: jnchung@ufl.eduw (J.N. Chung).

0960-8524/$ - see front matter © 2012 Elsevier Ltd. All rights reserved.
doi:10.1016/j.biortech.2011.12.105

and renewable biosyngas using a trailer-scale downdraft biomass gasification system.

Zainal et al. (2002) and Zainal et al. (2001) investigated gasification of four different biomass feedstock namely Wood, Paddyhusk, Paper and Municipal Waste. An equilibrium model was used to predict the Syngas composition and it was also used to visualize the variation in the syngas composition especially for H_2, CO and CH_4 with respect to the change in the moisture content of the feed stock, which in turn shows the trend in the calorific value of the different biomass materials as a function of the moisture content.

Gautam et al. (2010) used the equilibrium model approach to derive an expression that can predict the composition of the H_2, CO and CH_4 in the Syngas based on the C, H, O contents determined by the ultimate and proximate analysis for any type of biomass feedstock .The effect of gasification temperature on the composition of the syngas was also studied using the model. They also predicted the H_2 and CO contents for most common feedstock available in US using the model at 800 °C.

Sharma (2011a) performed experiments in a 75 KW downdraft gasifier system to analyze the fluid flow characteristics and thermo–chemical characteristics of the gasifier system. Overall pressure drop in the system in terms of the air/gas flow rate serves as a useful tool in coupling of gasifiers to gas engines which can provide a huge boost to power generation by decentralizing and using distributed power systems such as the trailer-scale units.

Karmakar and Datta (2011) studied gasification of rice husk experimentally and also developed an equilibrium model to predict the syngas composition. Although the authors used steam as the gasifying agent in their work, a similar equilibrium model approach which predicts the maximum achievable yield from the gasification system was developed. The work was based on the equilibrium constant method and does not include the complex mathematical formulations associated with the optimization methods.

Vera et al. (2011) evaluated the energy recovery potential for combined heat and power (CHP) system using a downdraft gasifier coupled with an externally fired gas turbine. Using olive waste as the feedstock, the system provides electricity on a scale down to 70 kW and thermal energy as sanitary hot water (about 160 kW). The plant is able to achieve an electric efficiency around 20% and overall efficiency around 65%.

Moon et al. (2011) did the economic analysis to compare two technologies of direct combustion using a steam turbine and gasification coupled with a syngas engine. For a small and distributed power generation system ranging from 0.5 to 5 MW_e, it was found that gasification with a syngas engine becomes more economically feasible as the plant size decreases. Regarding the cost of electricity generation, electrical efficiency and fuel cost significantly affect both direct combustion and gasification systems.

There are a lot of researchers who did experiments using the downdraft gasifier (Sheth and Babu, 2009; Martínez et al., 2011; Martínez et al., 2012; García-Bacaicoa et al., 2008; Centeno et al., 2012; Son et al., 2011) but only a few that used four different feedstock and even fewer captured the thermal profiles of the gasifier in different reaction zones for four different feedstock exclusively over the entire process. The present study discusses how the C, H, O content variations in the feedstock affect the thermal profiles in the different zones of the gasifier and their impact on the final syngas composition by using a thermodynamic equilibrium model that has been validated by comparison with other well known models. Additionally, this work also demonstrates the high efficiency and viability of a trailer-scale gasifier that is more useful for a single household located in a rural or remote area where biomass resource is plentiful for distributed energy applications.

2. Experimental setup and procedure

2.1. Trailer gasification system

The trailer-scale gasification system as shown in Fig. 1 was designed and built to emphasize on the effectiveness of distributed power generation systems and to demonstrate the feasibility of such gasification systems in real world scenarios, where the biomass resources are widely varying and distributed across the board. Fig. 2(a) shows the schematic of the gasifier design. The Imbert design downdraft gasifier (Reed and Das, 1988) has three main sections namely, the top hopper, the combustion and reduction chamber and the bottom ash chamber. The top hopper has a lid that facilitates the loading of the feedstock for operations and the mid-section has five radially arranged nozzles that are connected to a concentric chamber which in turn is connected to the main air intake valve on the outer surface that feeds the air into the gasifier. This design makes the gasifier self-adjusting on its own to compensate for excess coal or excess feedstock in the gasifier and automatically brings the reaction zone in line with the nozzles. The lower half of this section has the reduction chamber that incorporates the hour glass shape (Fig. 2) and additional thermal insulation, which highly improves the efficiency of the gasifier in breaking down the tar. The last section of the gasifier has the grate on which all the coal and feedstock are rested. This grate is controlled by a rotary shaker that helps prevent bridging in the reaction zone by constantly letting the ash settle down at the bottom.

The gasifier is connected to a syngas cleaning system as shown in Fig. 1. The exit of the gasifier is connected to a cyclone separator which helps in removing any particulates that gets carried along the syngas. After this the syngas enters the cooling tower that lowers the temperature of the gas significantly and makes it more energy dense and in the process it also condenses out tar vapor in the gas stream. The exit of the cooling tower is connected by a 2-way valve to the flare igniter which identifies the quality of the syngas by the flame color and once the flame changes from bright yellow to colorless fumes, the syngas is diverted to the two sets of filters (Fig. 1) that scrub the syngas clean of almost all the smaller particulates and remaining tars. Then the syngas is ready for use in a gas engine or can be sampled out for gas analysis.

2.2. Gas chromatograph

The gas composition analysis was done using a HP 5890AGas Chromatographer (GC) with a TCD column HP-PLOT 5A 30 m, 0.53 mm, 25 u. The GC was used to determine the constituent species based on the retention time in the gas column.

The chromatogram provides a spectrum of peaks for a sample representing the analytes present in a sample eluting from the column at different times. Retention time can be used to identify analytes if the method conditions are constant. Also, the pattern of peaks will be constant for a sample under constant conditions and can identify complex mixtures of analytes. The area under a peak is proportional to the amount of analytes present in the chromatogram. By calculating the area of the peak using the mathematical function of integration, the concentration of an analyte in the original sample can be determined. This area is then taken as the reference and known concentrations of the standards are used to determine the concentration of the gas sample. For each of the four runs samples were collected using air tight gas sampling bulbs via a gas port just after the filter exit to make sure that there were not any particulates or contaminants in the gas samples and also to make sure that the sample was not diluted. The sampling bulbs were purged approximately 5 times the normal volume before the stops were closed to secure the samples. The percentage differ-

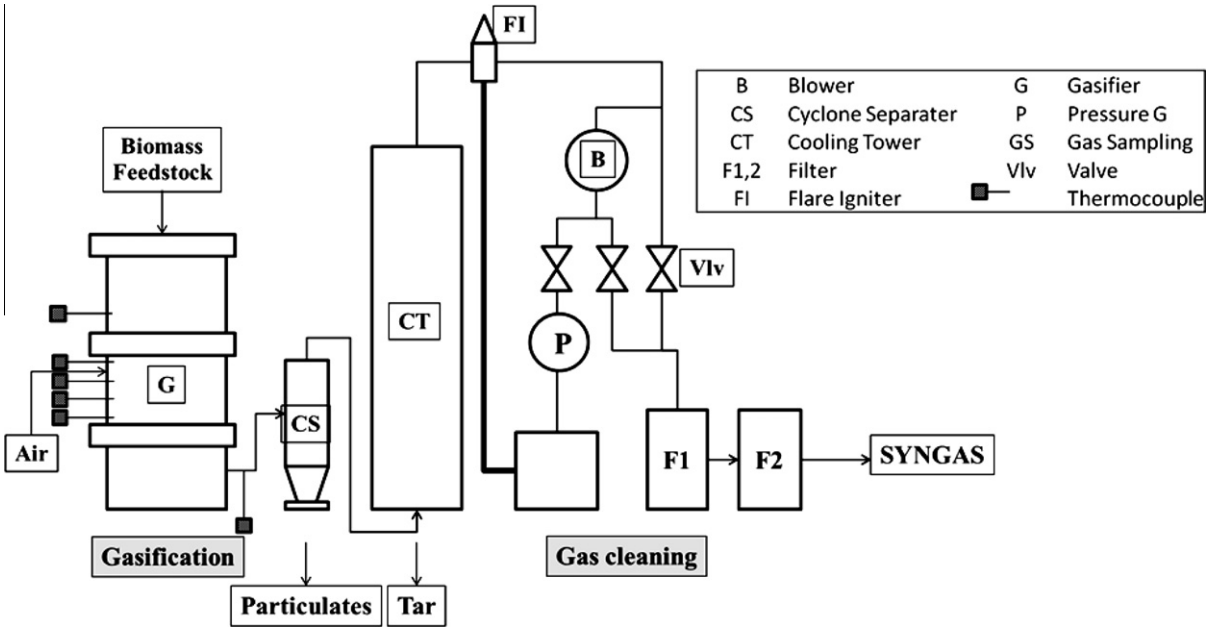

Fig. 1. Gasification unit and gas cleaning systemcomponents.

ences between the areas under the peak for the samples and standards for H_2 were between 0.006 and 1.307 and in case of CH_4 they were between 1.730 and 4.464, hence the concentrations determined using the standard are in the range of ±0.1% of the sample.

2.3. Experimental methods

To start the gasification process, measured amounts of coal is added to the grate filling it up to the level of the air intake nozzles. This serves as the heat source to overcome the thermal inertia of the gasifier and moderate the conditions suitable for gasification and also serves as the reduction zone for the gases passing through it during the reaction. Then the coal bed is ignited using a blow torch and the blower attached at the end of the gasifier is started to help pull the air through the gasifier to facilitate the combustion of coal and the variable speed blower settings are adjusted in such a way that it maintains a 5″ H_2O pressure differential across the throat of the gasifier, which is determined using the pressure monitor. The gasifier in the trailer system is equipped with K-type thermocouples at different zones of the reactor chamber to closely monitor the thermal gradient along the length of the gasifier as the reaction goes on and are continuously monitored using the DAQ system. Once the coal bed reaches the gasification temperature required, the amount of air flow into the system is controlled with the intake valve to maintain the reactor temperature.

After this the top hopper is opened and measured quantity of feedstock is added and the lid is closed tight. The grate motor is also turned on to prevent any bridging in the reactor. The exit gas temperature is also monitored continuously. When the temperature of the syngas exiting the gasifier reaches 250 °C, the igniter at the top of cooling tower is turned on to flare the syngas. The color of the flares provides an indication of the quality of gas produced and it is further processed tailoring the needs of the system. The flow rate of the syngas being produced is measured using a gas meter with movable diaphragms. Since it would be difficult to read the rotations of the needle in the meter manually the display was modified using an auto clicker that was connected to the needle using a relay and each rotation of the needle in the meter was recorded as a click in the counter and was used to determine the flow rate.

The same protocol was repeated for all four different feedstock and the temperatures were recorded at a 1s sampling rate. Pictorial representations of the TC locations are shown in Fig. 2(b). A similar approach to capture the thermal profile in the downdraft gasifier was used by Lu et al. (2007) but the sampling rate used was 2–3 min intervals. Any experimental measurement will involve some level of uncertainty that may originate from causes such as, inaccuracies in measurement equipment, random variables in quantity measured, and approximations in data. The uncertainties in the experiment are ±0.3%, ±0.1%, ±0.1%, ±0.2 in, ±0.1 in of H_2O, ±0.1% and ±0.01% for moisture content, weight measurement, temperature, feedstock size, pressure, ambient humidity and multimeter measurement, respectively. The experimental conditions and parameters are given in Table 1.

3. Numerical analysis

The thermal–chemical equilibrium model was tailored specifically to suit the downdraft gasifier, and the choice of the gasifier makes it less intense when it comes to the assumptions that were made to make the model reliable in predicting the syngas composition. To make the process of solving the simultaneous equations using computational methods the following assumptions were made,

1. The gasification reactor is in the thermodynamic equilibrium condition.
2. In the energy equation there is no heat loss term assuming that the system is perfectly insulated and there is no parasitic influence on the system i.e. the process is completely adiabatic.
3. Only C, H, O contents of the feedstock were chosen as in other literatures to validate the model, so other mineral contents were not considered because of the negligible amounts present.
4. The energy input provided by the coal bed to start-up the combustion reaction is not accounted for in the steady state overall energy balance. The charcoal added during the start-up of the experimental is intended for two purposes. The first is to get the combustion process going and the second is to heat up the entire system from room temperature to the gasification

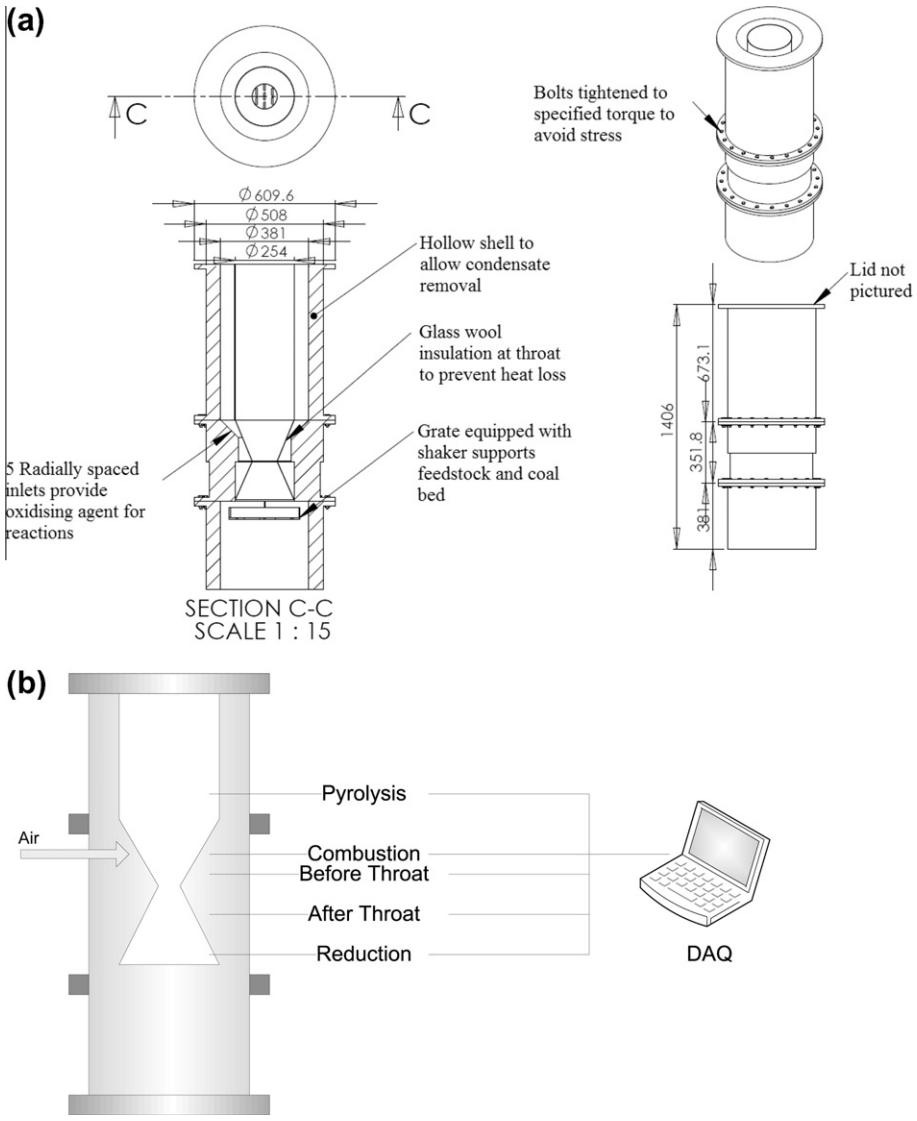

Fig. 2. (a) Schematic of the gasifier. (b)pictorial representation of thermocouple setup.

Table 1
Experimental conditions and parameters.

	Pine	Horse manure	Red oak	Cardboard
Test condition				
Ambient temperature [°C]	28.6	29.1	28.7	29.6
Relative humidity [%]	83.6	84.8	81.7	81.7
Moisture content[%]	12.2	18.33	14.8	12.6
Ultimate analysis [wt%] (Pettersson, 2009; Sorum et al., 2001)				
C	52.7	48.6	49.6	48.6
H	6.1	5.8	6.62	6.2
O	41.2	44.3	43.8	45
N	~	0.9	~	0.11
S	~	0.14	~	0.13
HHV [kJ/kg]	20,721	19,370	20,230	18,450
LHV [kJ/kg]	19,388	18,140	18,728	17,097
Feedstock loading [kg]	7.11	8.55	5.86	5.96
Charcoal loading [kg]	2.04	1.91	2.08	1.94
Air feed rate (m^3/h)	1290	1235	1326	1891
Syngas data				
Syngas flow rate [m^3/min]	0.57	0.65	0.68	0.71

temperature. As the gasification process reaches the steady state, part of the feedstock is consumed as the fuel in the combustion zone for a continuous gasification process.

5. All the Cs (solid carbon) is converted to syngas species and there is no solid carbon left after the gasification and the exit syngas is composed only of H_2, CO, CO_2, H_2O, CH_4 and N_2. Other higher Hydro carbons are neglected. The composition gases are modeled to exhibit ideal behavior irrespective of the high operating temperatures in the gasifier.
6. The syngas composition estimated is free of any O_2 from the supplied air since the amount of air supplied is constrained using the intake valve, making it a partial oxidation process and all the O_2 is consumed during the combustion reaction.

Global Equation:

$$CH_XO_Y + wH_2O + m(O_2 + 3.76 \cdot N_2) \Rightarrow a_1H_2 + a_2CO + a_3CO_2 + a_4H_2O + a_5CH_4 + m \cdot 3.76N_2 \quad (1)$$

The X and Y for the biomass feedstock are determined from the ultimate analysis of the feedstock. There are a total of 6 unknowns in this equation and the equilibrium calculations were carried out with H_2, CO, CO_2, H_2O, and CH_4 as the exit syngas components along with N_2. It is assumed that there is no soot formation and all the biomass is converted to the exit gas composition under a high temperature with no tar. The enthalpy changes of the product

gas constituents were calculated as a function of the gasification temperature using the fitted values given in NIST Chemistry WebBook (NIST, 2011) for corresponding constituents in specific temperature range.

Thus for solving the 6 unknowns, 6 simultaneous equations were formed using the data available from the global equation and the 2 independent reactions. The w is determined using the moisture content in the feedstock.

$$w = \frac{\mathrm{MW_{Bio}} * \mathrm{MC}}{\mathrm{MW_{H_2O}} * (1 - \mathrm{MC})} \tag{2}$$

$$\mathrm{CH_4 + H_2O \Longleftrightarrow CO + 3H_2} \quad \text{Methane reforming} \tag{3}$$

$$\mathrm{CO + H_2O \Longleftrightarrow CO_2 + H_2} \quad \text{Water gas shift} \tag{4}$$

The equations required for the numerical analysis are formulated using the C, H, O balance of the global equation followed by the rate constant equation for the 2 chemical equations considered and finally carrying out the energy balance for the whole system.

Carbon Balance:

$$a_2 + a_3 + a_5 - 1 = 0 \tag{5}$$

Hydrogen Balance:

$$2 \cdot a_1 + 2 \cdot a_4 + 4 \cdot a_5 - X - (2 \cdot w) = 0 \tag{6}$$

Oxygen Balance:

$$a_2 + 2 \cdot a_3 + a_4 - \mathrm{Y} - w - (2 \cdot m) = 0 \tag{7}$$

The equilibrium constant for methane decomposition can be written in terms of the moles of the participating species,

$$K_1 = \frac{[\mathrm{CO}] * [\mathrm{H_2}]^3}{[\mathrm{CH_4}] * [\mathrm{H_2O}]} \tag{8}$$

Similarly the equilibrium constant for water gas shift reaction can be written as,

$$K_2 = \frac{[\mathrm{CO_2}] * [\mathrm{H_2}]}{[\mathrm{CO}] * [\mathrm{H_2O}]} \tag{9}$$

These equilibrium constants are a function of the gasification temperature and they are described by following equations with coefficients given in Table 2.

$$C_p^\circ = A + B*t + \mathrm{C}*t^2 + D*t^3 + E/t^2 \tag{10}$$

$$H^\circ - H^\circ_{298.15} = A*t + B*t^2/2 + \mathrm{C}*t^3/3 + D*t^4/4 - E/t + F - H \tag{11}$$

$$S^\circ = A*\ln(t) + B*t + C*t^2/2 + D*t^3/3 - E/(2*t^2) + G \tag{12}$$

where C_p = heat capacity (J/mol∗K), H° = standard enthalpy (kJ/mol), S° = standard entropy (J/mol∗K) and t = temperature (K)/1000.Using the above values, the ΔH, ΔS, ΔG for the equilibrium reactions were calculated as given below,

$$\Delta H_1 = (3 \cdot h_{H_2} + h_{\mathrm{CO}} - h_{\mathrm{H_2O}} + h_{\mathrm{CH_4}}) \tag{13}$$

$$\Delta \mathrm{H}_2 = (h_{\mathrm{CO_2}} + h_{H_2}) - (h_{\mathrm{CO}} + h_{\mathrm{H_2O}}) \tag{14}$$

$$\Delta S_1 = (3 \cdot S_{H_2} + S_{\mathrm{CO}}) - (S_{\mathrm{H_2O}} + S_{\mathrm{CH_4}}) \tag{15}$$

$$\Delta S_2 = (S_{\mathrm{CO_2}} + S_{H_2}) - (S_{\mathrm{CO}} + S_{\mathrm{H_2O}}) \tag{16}$$

$$\Delta G_1 = \Delta H_1 - (\Delta S_1/1000) \cdot (t \cdot 1000) \tag{17}$$

$$\Delta G_2 = \Delta H_2 - (\Delta S_2/1000) \cdot (t \cdot 1000) \tag{18}$$

$$K_1 = \exp\left(\frac{-\Delta G_1}{8.3 * t}\right) \tag{19}$$

$$K_2 = \exp\left(\frac{-\Delta G_2}{8.3 * t}\right) \tag{20}$$

So now, the K values are written in terms of the unknown values as per definition, and the Gibbs free energy technique is used to set up the variables in terms of the equilibrium constants.

$$K_1 = (a_1^3 * a_2/a_5 * a_4) \times \left(4/(a_1 + a_2 + a_3 + a_4 + a_5 + 3.76 * m)^2\right) \tag{21}$$

$$K_2 = a_1 * a_3/a_2 * a_4 \tag{22}$$

$$Q - W = \sum n\mathrm{H_{out}} - \sum n\mathrm{H_{in}} \tag{23}$$

The energy equation can be written in detail as follows, with the reference temperature is 298 K and pressure is 1 atm.

$$\begin{aligned} H^0_{fBio} + w * (H^0_{f_{H_2O}} + H_{vap}) + m * (H^0_{f_{O_2}} + 3.76 * H_{f_{N_2}}) \\ = a_1 * (H^0_{f_{H_2}} + \int_{T_0}^{T_G} C_{pH_2} dT) + a_2 * (H^0_{fCO} + \int_{T_0}^{T_G} C_{pCO} dT) + a_3 \\ * (H^0_{f_{CO_2}} + \int_{T_0}^{T_G} C_{p_{CO_2}} dT) + a_4 * (H^0_{f_{H_2O}} + \int_{T_0}^{T_G} C_{p_{CO_2}} dT) + a_5 \\ * (H^0_{f_{CH_4}} + \int_{T_0}^{T_G} C_{p_{CH_4}} dT) + m * 3.76 * (H^0_{f_{N_2}} + \int_{T_0}^{T_G} C_{p_{N_2}} dT) \end{aligned} \tag{24}$$

Owing to the complexities in solving the equations, a mathematical solver MAPLE was used to carry out the calculations and determine the exit syngas composition. The model was run for all the four different feedstock with their respective properties accounted for. Reliability of the model was also tested by using input conditions from other similar literature works and comparing the results with various models for validation.

4. Results and discussions

4.1. Gasifier thermal characteristics

The detailed temperature profiles inside the gasifier are shown in Figs. 3–5 for the five zones of pyrolysis, combustion, before throat, after throat and reduction with all the four different feedstock included for comparison. The legends have been placed at certain distance percentage on the temperature curve to make it very readable, since the data points were collected at a sampling rate of 1 s.

A general trend found on all the temperature history profiles is the oscillations. They are mainly in the combustion and pyrolysis zones. The main reason for the oscillations is the self-regulating

Table 2
A, B, C, D, E, F, G, H for individual species from NIST Chemistry webBook (NIST, 2011).

Species	H_2	CO	CO_2	$H_2O_{(g)}$	CH_4	$H_2O_{(l)}$
A	18.5631	25.56759	24.99735	30.092	−0.70303	−203.606
B	12.2574	6.09613	55.18696	6.832514	108.4773	1523.29
C	−2.8598	4.054656	−33.6914	6.793435	−42.5216	−3196.413
D	0.26824	−2.6713	7.948387	−2.53448	5.862788	2474.455
E	1.97799	0.131021	−0.13664	0.082139	0.678565	3.855326
F	−1.1474	−118.009	−403.608	−250.881	−76.8438	−256.5478
G	156.288	227.3665	228.2431	223.3967	158.7163	−488.7163
H	0	−110.527	−393.522	−241.826	−74.8731	−285.8304

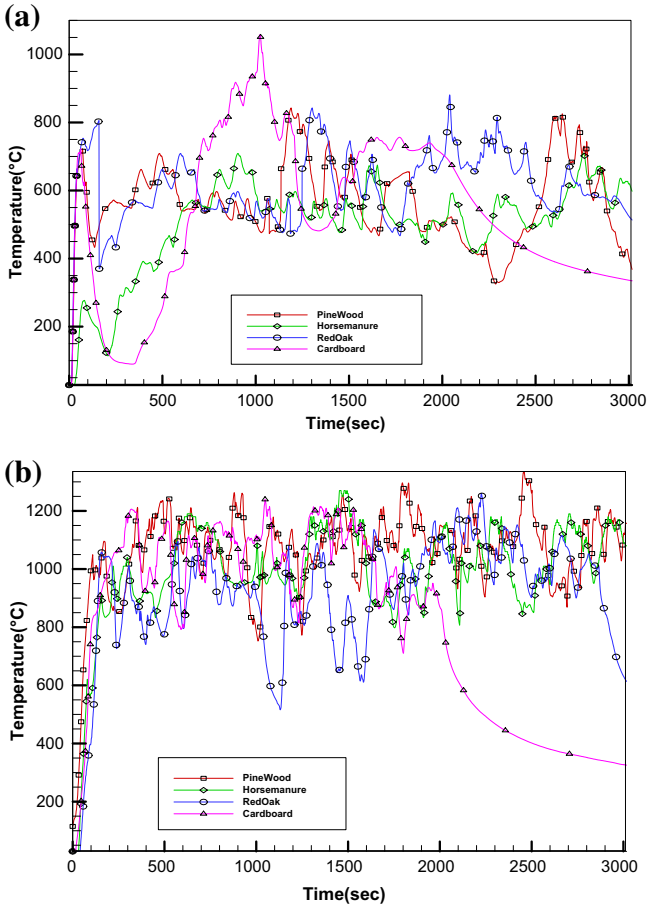

Fig. 3. Temperature histograms. (a) pyrolysis zone, (b) combustion zone.

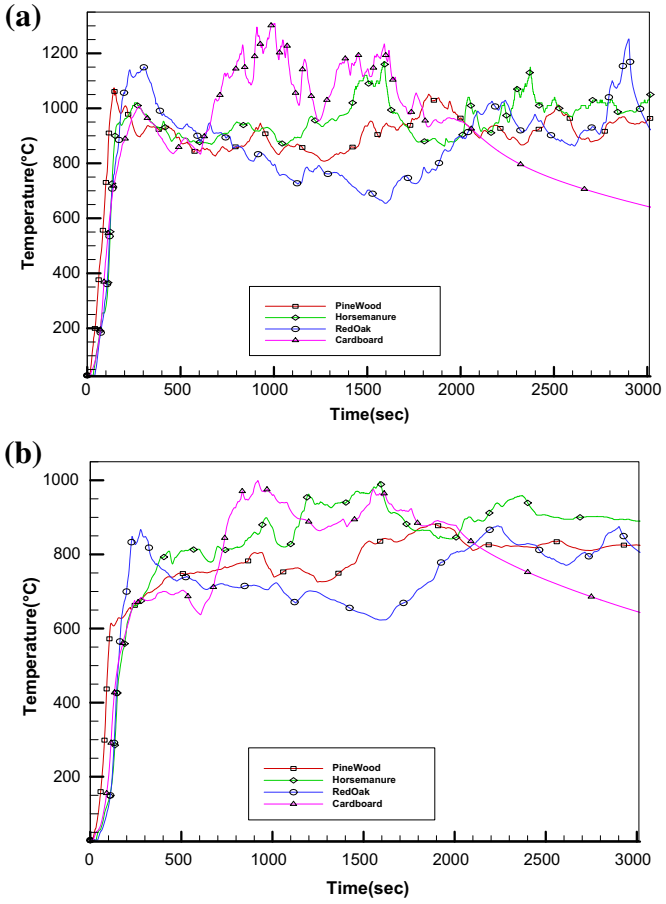

Fig. 4. Temperature histogram. (a) before throat. (b)after throat.

nature of the downdraft gasifier mentioned above. The oscillations are believed to be attributed to the alternating sequence between the air intake flow and the flu gas flow. First the cycle starts when the air flow must be cranked up to facilitate the combustion and the production of flue gas that then rises up to the pyrolysis zone. The flu gas then recirculates back down once it loses heat to the feedstock for pyrolysis and as it reenters the combustion zone it retards the intake air flow. As a result, the combustion slows down and so does the flu gas production that will cause the flu gas flow rate to decrease and the air flow to increase to support more combustion and that starts a new cycle.

The pyrolysis zone profiles given in Fig. 3(a) show a very high peak at 1000 s for the cardboard feedstock, this may be because of the low density nature of the feed stock which tends to form localized pockets filled with air in the gasifier which when exposed to the reaction zone as gasification progresses will release a lot of heat because of the sudden inclusion of the oxidizing agent. Although other feedstock also shows similar isolated high peaks but they are all lower than that of cardboard because of their inherently high density distributions in the hopper with lower number of air pockets. In Fig. 3(b), the combustion Zone temperature profiles display some high-frequency fluctuations which were captured because of the high sampling rate. The reasons for such large fluctuations in this zone are explained by (Lu et al., 2007) but these authors actually showed a fairly smooth profile with minimal fluctuations in the combustion zone in their results which they attributed to a low sampling rate. Usually a low sampling rate damps out the jumps in the combustion zone especially. This is the zone where all the heat required for the gasification reaction is produced and hence the temperatures are the highest among all five zones.

Figs. 4 and 5(a) basically represent the 3 zones that make up the space between the throat of the gasifier and the grate which is primarily the region where all the tar cracking and reformation reactions take place. The average temperature peaks in this region drop to 800 °C from 1100 °C and it is mainly because of the endothermic nature of the reactions that take place in the reduction zone.

Fig. 5(b) shows the temperature history curves for all the five zones in the gasifier using horse manure as the feedstock and it can be seen clearly from the profiles that the reaction zones near the throat are more stable with much smaller fluctuation amplitudes and frequencies than the combustion and pyrolysis zones, which is attributed to the fluctuations in heat releases due to interaction with O_2 trapped in the hopper section, and the average temperature in the reduction process is 850 °C which is high enough to crack tar and facilitate shift and reformation reactions.

The time-averaged temperatures are plotted in Fig. 6 for each zone and all four feedstock where Zones 0, 1, 2, 3, and 4 represent pyrolysis, combustion, before throat, after throat and reduction zones, respectively. Generally the combustion zone, as expected, has the highest average temperature, followed by before the throat zone, after the throat zone and reduction zone. The pyrolysis zone has the lowest temperature. The trends shown in Fig. 6 are consistent and similar with those given by (Olgun et al., 2011). It clearly shows that all the four feedstock display almost similar trends in all the 5 zones.

4.2. Model simulation results

In order to check the validity of the current model developed specifically for the current trailer gasifier, the model predictions

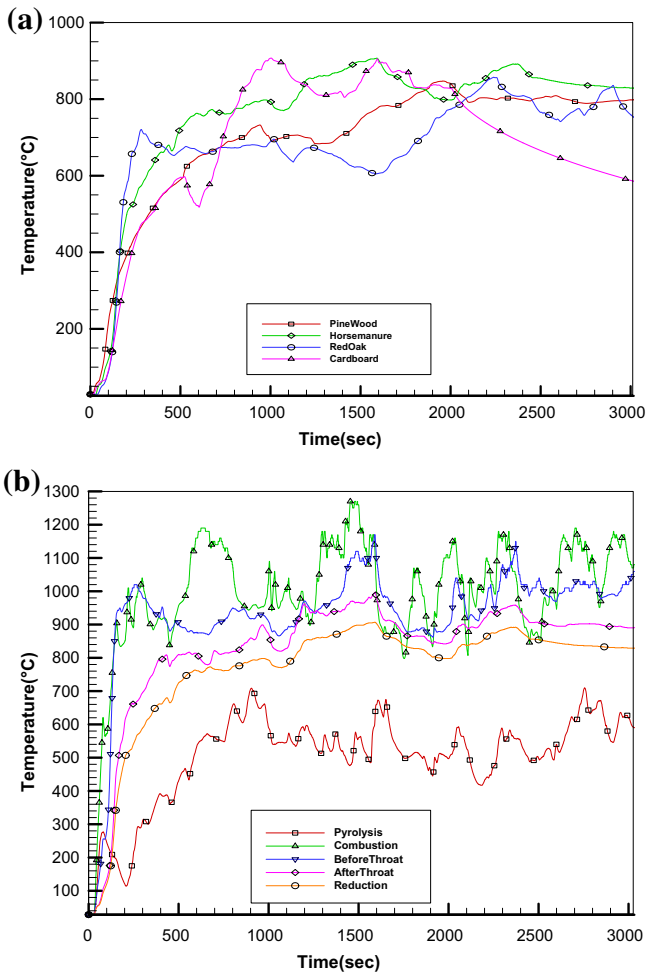

Fig. 5. Temperature histograms, (a) reduction zone, (b) all zones for horse manure.

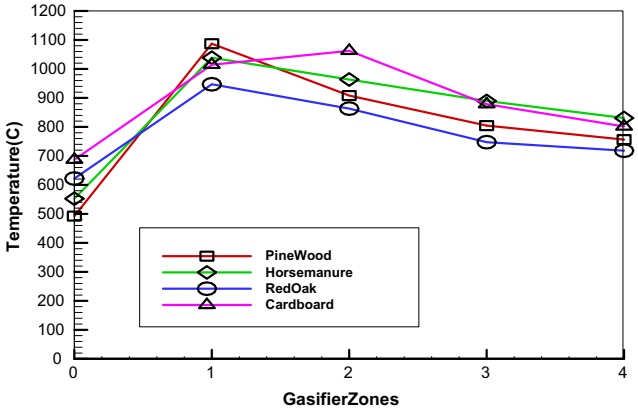

Fig. 6. Time-average temperatures in each zone for all four feedstock.

were compared to other well known models widely used in the literature and the results are tabulated in Table 3. For making the comparisons easier the models used by the corresponding authors have been named as follows.

Model 1 GasifEq (Mountouris et al., 2006).
Model 2 GasEq (Morley, 2005).
Model 3 ChemEq (Sandler, 1999).
Model 4 Predicted (Zainal et al., 2001).
Model 5 SynGas model (Altafini et al., 2003).
Model 6 Cycle-Tempo model (Altafini et al., 2003).

The chemical properties from NIST Chemistry WebBook (NIST, 2011) have been used in this study whereas the other authors have used values from Chemical Properties Handbook (Yaws, 1999). Since the equilibrium constant is very sensitive to the coefficients, any slight change in the chemical composition of syngas is attributed to the use of different standards for calculating them, which is clearly shown next. For the reaction of $CO + H_2O = CO_2 + H_2$ at 1273 K, the equilibrium reaction constants used in Models 1, 2, 3 and the current model are 0.558, 0.607, 0.56, 0.604 respectively. While for $CH_4 + H_2O = CO + 3H_2$ at 1273 K, the reaction constants are 8835, 8861, 8624 and 9251 for Models 1, 2, 3, and the current model, respectively. Lastly, for $C + H_20 = CO + H_2$ at 1273 K, the reaction constants are 94.7, 82.7, 82.6 and 95.6 for Models 1, 2, 3, and current model, respectively.

The gasifier output gas compositions predicted by the current model at 1073 K with moisture contents of 10% and 20% under no heat condition for wood waste are given in Table 3 that also lists the results from other models for comparison. Although the syngas compositions predicted by the current model is in accordance with other literature values, the variations in the syngas composition shown in Table 3are mainly due to the following reasons: the type of independent reactions chosen for solving the model and the enthalpy of formation of wood. For the enthalpy of formation, it was taken to be 149.752 kJ/mol by (Mountouris et al., 2006) in their model whereas a value of 118.050 kJ/mol was used by (Zainal et al., 2001) and (Altafini et al., 2003),which is due to the error in using the enthalpy of formation of water vapor instead of liquid water as explained by these authors. But in the current model the enthalpy of formation was calculated for the different feed stock based on their compositions.

Now using the experimental input conditions for our four different feedstock materials and using the ultimate analysis to determine the heat of formation and number of moles of water from the moisture content of each feedstock, the current model was applied to predict the syngas compositions and the details of the volumetric composition and the heating values of the syngas are listed in Table 4.

4.3. Gasifier efficiency

In this section, the thermodynamic efficiency of the current trailer-scale gasification system is first estimated using the results from the equilibrium thermal–chemical conversion model presented in the previous section and then verified by using the experimental data of syngas composition. The thermodynamic efficiency of the gasifier is calculated using the ratio of the calorific value of the syngas to that of the respective biomass feedstock as shown below.

$$\eta_{\text{gasifier}} = \frac{\text{Calorific value of syngas per mol}}{\text{Calorific value of 1 mol of feedstock}} \quad (25)$$

The calorific value of the feedstock was selected for each feedstock from Table 1 and the calorific value of syngas was obtained from the LHV of the syngas that is listed in Table 4. Both calorific values and the efficiency for each feedstock are given in Table 5. The efficiencies calculated for the four feedstock are in the range of 80%. The efficiencies for the current four feedstock are in good agreement with the values determined by several other researchers for similar gasifiers (Sharma, 2008; Sharma, 2011b; Goswami

Table 3
Various model predictions of syngas compositions with 10% or 20% moisture content at 1073 K under no heat added using wood waste.

20% Moisture gas comp.% v/v	Model 1	Model 4	Current model	
H_2	18.44	21.06	20.13256	
CO	17.46	19.61	18.51965	
CO_2	13.13	12.01	12.79253	
CH_4	0	0.64	0.01689	
N_2	50.96	46.68	48.53837	
Total	100	100	100	
10% Moisture gas comp% v/v	Model 1	Model 5	Model 6	Current Model
H_2	19.8	20.06	21.4	18.51988
CO	23.45	19.7	23	20.78001
CO_2	9.16	10.15	9.74	11.11706
CH_4	0.01	0	0.01	0.02411
N_2	47.57	50.1	45.31	49.55895
Total	100	100.01	99.56	100

Table 4
Syngas composition estimated from our current model at 1173 K, no heat added. Bold terms indicate the total heating values.

Feedstock	Species	N	MW g/mol	Vol%	M	Wt%	Species LHV MJ/kg	Syngas LHV MJ/kg
Pine	H_2	0.7011	2	20.20	1.40	1.76	120.00	2.11
	CO	0.6842	28	19.71	19.16	23.98	10.10	2.42
	CO_2	0.3157	44	9.10	13.89	17.39		0.00
	H_2O	0.4117	18	11.86	7.41	9.28		0.00
	CH_4	9E-05	16	0.00	0.00	0.00	50.00	0.00
	N_2	1.3583	28	39.13	38.03	47.60		0.00
Total		3.47		100.00	79.90	100.00		**4.53**
Horse	H_2	0.6909	2	21.90	1.38	1.93	120.00	2.32
Manure	CO	0.7326	28	23.22	20.51	28.71	10.10	2.90
	CO_2	0.2673	44	8.47	11.76	16.46		0.00
	H_2O	0.3207	18	10.16	5.77	8.08		0.00
	CH_4	0.0001	16	0.00	0.00	0.00	50.00	0.00
	N_2	1.1437	28	36.25	32.02	44.82		0.00
Total		3.16		100.00	71.45	100.00		**5.22**
Red	H_2	0.748	2	22.17	1.50	1.97	120.00	2.37
Oak	CO	0.721	28	21.37	20.19	26.64	10.10	2.69
	CO_2	0.2788	44	8.27	12.27	16.19		0.00
	H_2O	0.3681	18	10.91	6.63	8.74		0.00
	CH_4	0.0001	16	0.00	0.00	0.00	50.00	0.00
	N_2	1.2576	28	37.28	35.21	46.46		0.00
Total		3.37		100.00	75.80	100.00		**5.06**
Cardboard	H_2	0.6452	2	18.57	1.29	1.58	120.00	1.89
	CO	0.6688	28	19.25	18.73	22.91	10.10	2.31
	CO_2	0.3311	44	9.53	14.57	17.83		0.00
	H_2O	0.4065	18	11.70	7.32	8.95		0.00
	CH_4	7E-05	16	0.00	0.00	0.00	50.00	0.00
	N_2	1.4225	28	40.94	39.83	48.73		0.00
Total		3.47		100.00	81.74	100.00		**4.21**

Table 5
Thermodynamic efficiency based on equilibrium model.

	Pine	Horse manure	Red oak	Cardboard
LHV Syngas MJ/mol	0.361830837	0.373108683	0.383532315	0.3440523471
LHV feedstock MJ/mol	0.44147249	0.44207851	0.45318745	0.42130393
Gasifier efficiency	0.819599973	0.843987375	0.84629951	0.816636924

1986). The average value for the gasifier efficiency using woody biomass types in a downdraft system is about 75% but it could be as high as 90% in some special cases.

It should be pointed out that even though the above thermodynamic efficiency values are calculated based on the syngas compositions predicted by the current equilibrium model, the following supporting evidence would suggest that the actual efficiencies of the current trailer-scale gasifier should be very close to those predicted values listed in Table 5. Table 6 provides a comparison between our experimental data and those predicted by the current equilibrium model for the hydrogen volume percent in the syngas. The differences between the two sets of results are explained below.

1. The assumptions listed in Section 3. Numerical analysis may not take place totally during the experiment especially the equilibrium and adiabatic conditions that usually result in a higher hydrogen volume fraction.
2. The model prediction is based on the reactor temperature of 1173 K while the actual gasifier has variations both in space and in time as seen in Figs. 3–6.
3. As a result of the temperature variations, some tar would form in the experimental gasifier due to low temperature spots while no tar formation was assumed in the model.
4. The deviation between the values from the model and experiment is relative large for the cardboard that may be due to its much lower density. The lower density feedstock tends to

Table 6
Syngas composition from experiments.

	Pine		Horse manure		Red oak		Cardboard	
	H_2	CH_4	H_2	CH_4	H_2	CH_4	H_2	CH_4
Experimental value volume%	15	5	20	3	17	1.5	11	3
Model prediction volume%	20.20	0	21.90	0	22.17	0	18.57	0

entrain more air due to loose pockets. The ultimate analysis values selected from the literature may not fit directly to the type of cardboard that was used in the current study.

5. All the models in the literature under estimated the CH_4 content in the syngas because the models do not take in to account the amount of CH_4 produced from cracking of tar and other volatiles which is basically the case in an actual gasifier.

With considerations given to the differences between the model assumptions and the actual experimental conditions and also the experimental uncertainties, the agreement shown in Table 6 between the experiment and the model is reasonably good except for the cardboard. Based on the relatively close comparison, it is suggested that the current trailer-scale distributed energy gasification system would be capable of delivering the efficiencies predicted by the model for a variety of feedstock.

4.4. Practical application

Many published papers have presented theoretical, analytical and experimental investigations on the integration of the gasifier with a power production device. For medium to large-scale gasifiers, gas turbines are considered the best choice (Aravind et al., 2009; Baratieri et al., 2009) while for small-scale gasifiers, a Stirling engine or an IC engine/generator set is the optimal selection. Lin (2007) investigated the integration of an updraft fixed bed gasifier with a Stirling engine, and the combined system successfully generated 24.5 kW shaft power. Shah et al. (2010) focused on the engine performance and emission of a 5.5 kWe spark-ignited engine operated by the syngas produced using a fixed bed, downdraft atmospheric pressure gasifier fed with hardwood chips. Centeno et al. (2012) presented a theoretical and experimental investigation of a downdraft biomass gasifier-spark ignition engine combined power system. They demonstrated the feasibility and practical application of the coupled system with up to 10 kW electrical power output. For the gasifier investigated in the current paper, an estimate was made based on the papers mentioned above and the result shows that if it were coupled with an 1800 rpm IC engine/generator set, the system would generate an average electrical power output of 11 kW with the four feedstock materials used in the current paper. The entire combined system of the gasifier with the engine/generator set would easily fit on a trailer of 4×2 m in size that can be towed by a small pick-up truck. This 11 kWe gasifier-engine system can be used for many practical purposes such as on a farm, in rural areas or for emergency power during nature disasters.

5. Conclusion

The feasibility and viability of a trailer-scale thermal–chemical system for the conversion of lignocellulosic biomass to biofuels have been demonstrated for distributed energy and rural applications. A thermodynamic equilibrium model that is capable of predicting the gasifier performance has been developed and validated by independent models in open literature. The current experimental results provided the system thermal profiles and quantitative hydrogen production rates. The thermodynamic efficiencies predicted by the model and backed by our experimental data are in the range of lower 80% for the four different feedstock used in this study that is in good agreement with other reports on gasification.

Acknowledgements

Funding for this research was provided by the Florida Institute for Sustainable Energy (FISE) and the Florida Energy Systems consortium (FESC).

References

Altafini, C.R., Wander, P.R., Barreto, R.M., 2003. Prediction of the working parameters of a wood waste gasifier through an equilibrium model. Energ. Convers. Manage. 44, 2763–2777.
Aravind, P.V., Woudstra, T., Woudstra, N., Spliethoff, H., 2009. Thermodynamic evaluation of small-scale systems with biomass gasifiers, solid oxide fuel cells with Ni/GDC anodes and gas turbines. J. Power. Source. 190, 461–475.
Baratieri, M., Baggio, P., Bosio, B., Grigiante, M., Longo, G.A., 2009. The use of biomass syngas in IC engines and CCGT plants: a comparative analysis. Appl. Thermal Eng. 29, 3309–3318.
Centeno, F., Mahkamov, K., Silva Lora, E.E., Andrade, R.V., 2012. Theoretical and experimental investigations of a downdraft biomass gasifier-spark ignition engine power system. Renew. Energ. 37, 97–108.
Corradetti, A., Desideri, U., 2007. Should biomass be used for power or hydrogen production? J. Eng. Gas Turbines Power 129, 629–636.
García-Bacaicoa, P., Mastral, J.F., Ceamanos, J., Berrueco, C., Serrano, S., 2008. Gasification of biomass/high density polyethylene mixtures in a downdraft gasifier. Bioresour. Technol. 99, 5485–5491.
Gautam, G., Adhikari, S., Bhavnani, S., 2010. Estimation of biomass synthesis gas composition using equilibrium modeling. Energ. Fuels 24, 2692–2698.
Goswami, Y., 1986. Alternative Energy in Agriculture, Vol. II, CRC Press, 83–102.
Huber, G.W., 2007. Breaking the chemical and engineering barriers to lignocellulosic biofuels: A research roadmap for making lignocellulosic biofuels a practical Reality, NSF, DOE and American Chemical Society Workshop.
Karmakar, M.K., Datta, A.B., 2011. Generation of hydrogen rich gas through fluidized bed gasification of biomass. Bioresour. Technol. 102, 1907–1913.
Lin, J.M., 2007. Combination of a biomass fired updraft gasifier and a stirling engine for power production. J. Energ. Resour. Technol. 129, 66–70.
Lu, P., Yuan, Z., Ma, L., Wu, C., Chen, Y., Zhu, J., 2007. Hydrogen-rich gas production from biomass air and oxygen/steam gasification in a downdraft gasifier, Renew. Energy 32, 2173–2185.
Martínez, J.D., Silva Lora, E.E., Andrade, R.V., Jaén, R.L., 2011. Experimental study on biomass gasification in a double air stage downdraft reactor. Biomass Bioenerg. 35, 3465–3480.
Martínez, J.D., Mahkamov, K., Andrade, R.V., Silva Lora, E.E., 2012. Syngas production in downdraft biomass gasifiers and its application using internal combustion engines. Renew. Energ. 38, 1–9.
Moon, J., Lee, J., Lee, U., 2011. Economic analysis of biomass power generation schemes under renewable energy initiative with Renewable Portfolio Standards (RPS) in Korea. Bioresour. Technol. 102, 9550–9557.
Morley, C., 2005. GasEq. Chemical equilibria in perfect gases. Version 0.78, Available from: www.gaseq.co.uk.
Mountouris, A., Voutsas, E., Tassios, D., 2006. Solid waste plasma gasification: Equilibrium model development and exergy analysis. Energ. Convers. Manage. 47, 1723–1737.
NIST, 2011. Chemistry WebBook. http://webbook.nist.gov/chemistry/.
Olgun, H., Ozdogan, S., Yinesor, G., 2011. Results with a bench scale downdraft biomass gasifier for agricultural and forestry residues. Biomass Bioenerg. 35, 572–580.
Pettersson, E., 2009. Combustion of horse manure for heat production. Bioresour. Technol. 100, 3121–3126.
Reed, T.B., Das, A., 1988. Handbook of Biomass Downdraft Gasifier Engine Systems, SERI/SP-271-3022, U.S. Department of Energy publication.
Ruan, R., Chen, P., Hemmingsen, R., Morey, V., Tiffany, D., 2008. Size matters: small distributed biomass energy production systems for economic viability, Int. J. Agric. Biol. Eng. 1, 64–68.
Sandler, S.I., 1999. ChemEq. Equilibrium model, In: Chemical and Engineering Thermodynamics, 3rd edition. John Wiley and Sons.

Shah, A., Srinivasan, R., To, S.D.F., Columbus, E.P., 2010. Performance and emissions of a spark-ignited engine driven generator on biomass based syngas. Bioresour. Technol. 101, 4656–4661.

Sharma, A.K., 2008. Equilibrium modeling of global reduction reactions for a downdraft (biomass) gasifier. Energ. Convers. Manage. 49, 832–842.

Sharma, A.K., 2011a. Experimental investigations on a 20 kWe, solid biomass gasification system. Biomass Bioenerg. 35, 421–428.

Sharma, A.K., 2011b. Modeling and simulation of a downdraft biomass gasifier 1. Model development and validation. Energ. Convers. Manage. 52, 1386–1396.

Sheth, P.N., Babu, B.V., 2009. Experimental studies on producer gas generation from wood waste in a downdraft biomass gasifier. Bioresour. Technol. 100, 3127–3133.

Son, Y., Yoon, S.J., Kim, Y.K., Lee, J., 2011. Gasification and power generation characteristics of woody biomass utilizing a downdraft gasifier. Biomass Bioenergy. 35, 4215–4220.

Sorum, L., Gronli, M.G., Hustad, J.E., 2001. Pyrolysis characteristics and kinetics of municipal solid wastes. Fuel 80, 1217–1227.

Vera, D., Jurado, F., Carpio, J., 2011. Study of a downdraft gasifier and externally fired gas turbine for olive industry wastes. Fuel Process Technol. 92, 1970–1979.

Yaws, C.L., 1999. Chemical Properties Handbook. McGraw-Hill, New York.

Zainal, Z.A., Ali, R., Lean, C.H., Seetharamu, K.N., 2001. Prediction of performance of a downdraft gasifier using equilibrium modeling for different biomass materials. Energ. Convers. Manage. 42, 1499–1515.

Zainal, Z.A., Rifau, A., Quadir, G.A., Seetharamu, K.N., 2002. Experimental investigation of a downdraft biomass gasifier. Biomass Bioenerg. 23, 283–289.